Unsaturated Soils – Alonso & Gens (eds)
© 2011 Taylor & Francis Group, London, ISBN 978-0-415-60428-4

Non-isothermal infiltration in plastic bentonite

B. François
Université de Liège, Departement ArGEnCo, Chemin des Chevreuils, Belgium
FRS-FNRS, Fonds National de la Recherche Scientifique, Bruxelles, Belgium

L. Laloui
Laboratory of Soil Mechanics (LMS), Ecole Polytechnique Fédérale de Lausanne (EPFL), Lausanne, Switzerland

ABSTRACT: In deep geological repository involving a multi-barrier system, the engineered materials, generally made of bentonite, constitute an important mechanical, thermal and hydraulic barrier to prevent the interaction between wastes and biosphere. To better understand the THM (thermo-hydro-mechanical) processes in the clayey confining system, experimental tests must be simulated by the means of advance numerical tools. A unified thermo-mechanical constitutive model for unsaturated soils, ACMEG-TS, has been developed and implemented in the finite element code LAGAMINE. Material is considered as tri-phase non-isothermal thermo-plastic medium. The results of numerical simulations of non-isothermal infiltration tests through FEBEX bentonite are compared with the available sensors measurements and interpreted in the light of elasto-thermo-plasticity of unsaturated soils. Through those simulations, the advancements in the understanding of the involved processes brought by the ACMEG-TS model are discussed.

1 INTRODUCTION

In the coming years, safe and definitive solutions will likely be completed for managing the large quantities of high-level radioactive wastes that stem mainly from nuclear electricity production. Deep geological repositories constitute one of the most promising options to isolate such wastes from the human environment. In this context, the highly coupled thermo-hydro-mechanical (THM) phenomena that occur in the engineered and geological barriers must be captured adequately by means of numerical analysis (Laloui et al., 2008). To validate and calibrate the mathematical models, numerical simulations of in-situ experiments reproducing analogue studies have to be performed.

As a preliminary test of a large scale in-situ test (FEBEX), Lloret et al. (2004) designed and carried out a non-isothermal infiltration test through the bentonite inside cylinders that aim at simulating the water that saturates the barrier in a repository. This experimental test encompasses the main THM processes that must be considered in numerical predictions of the behaviour of an engineered barrier for nuclear waste disposal.

The paper presents, first, the mathematical formulation of the used constitutive and numerical tools and the calibration of the material parameters of the FEBEX bentonite. Then, the features of the performed numerical analysis are presented and the comparison between obtained results and in-situ measurements is discussed. Finally, we interpret the obtained results in terms of mechanical irreversibilities, coupling between mechanical, thermal and water retention responses and diffusion processes.

2 THEORETICAL FORMULATION

2.1 *Equilibrium and balance equations*

The balance equations are obtained by considering that the material is composed of solid matrix and voids filled with liquid and gas phases. The liquid phase is assumed to contain two species: liquid water and dissolved air. Similarly, the gas phase is composed of dry air and water vapour. To uniquely describe the state of the material, four primary state variables are needed: gas pressure p_g, water pressure p_w, temperature T, and solid displacement vector $\mathbf{u}$. The solid phase component is assumed to be deformable while the water phase is slightly compressible. The solid, liquid, and water phases are assumed in thermal equilibrium, and a unique temperature is defined at each node.

The mass balances are described for the components (also called species) present in the mixture rather than for the phases. Therefore, the conservation of mass of each chemical species (water

and air) is assumed. The equilibrium and balance equations, as well as the water and heat flows, are expressed in the moving current configuration through a Lagrangian actualised formulation. The Lagamine finite element code including the three-phase field equations described above has been used (Charlier et al., 2001). The governing equations (solid, liquid, gas and energy balance equations) are presented in Collin et al. (2002), Collin (2003) and Collin et al. (2006).

2.2 *Constitutive relations*

The conservation equations which govern the THM equilibrium of the system need to be expressed in terms of the primary state variables (**u**, p_w, p_g, and T), after introduction of the constitutive relationships detailed below. The liquid water bulk density depends on the pore water pressure p_w and temperature T through the water bulk modulus χ_w and the volumetric water thermal expansion coefficient β'_w:

$$\rho_w = \rho_{w0}\left(1+\frac{p_w - p_{w0}}{\chi_w} - \beta'_w\left(T-T_0\right)\right) \tag{1}$$

where ρ_{w0}, p_{w0}, and T_0 are the initial values of water bulk density, pore water pressure, and temperature, respectively. The bulk density of the water vapour is determined through the following equation:

$$\rho_v = \exp\left(\frac{\left(p_w - p_g\right)M_v}{R\,T\rho_w}\right)\frac{p_{v,0}M_v}{R\,T} \tag{2}$$

where p_g is the gas pressure, M_v is the vapour molar mass (= 0.018 kg/mol), R is the constant of perfect gases (8.3143 J/(mol.K), ρ_w is the bulk density of liquid water, T is temperature expressed in Kelvin. The saturated vapour pressure $p_{v,0}$ is given by:

$$p_{v,0} = a\exp\left(-b/T\right) \tag{3}$$

with a = 112659MPa and b = 5192.74K for temperature range between 273 K and 373 K.

The gas phase is assumed to be an ideal gas in agreement with the Dalton law:

$$p_g = p_a + p_v \tag{4}$$

Consequently, the bulk density of dry air is:

$$\rho_a = \frac{p_a M_a}{R\,T} = \frac{\left(p_g - p_v\right)M_a}{R\,T} = \frac{p_g M_a}{R\,T} - \frac{\rho_v M_a}{M_v} \tag{5}$$

where M_a is the dry air molar mass (= 28.8 10^{-3} kg/mol) and ρ_v the bulk density of water vapor.

The velocity of liquid and gas phases are governed by the generalized Darcy's law:

$$\mathbf{f_l} = -\frac{\mathbf{k_w}}{\mu_w}\left(\mathbf{grad}\left(p_w\right) + g\rho_w\mathbf{grad}\left(y\right)\right) \tag{6}$$

$$\mathbf{f_g} = -\frac{\mathbf{k_g}}{\mu_g}\left(\mathbf{grad}\left(p_g\right) + g\rho_g\mathbf{grad}\left(y\right)\right) \tag{7}$$

where $\mathbf{k_w}$ and $\mathbf{k}_g$ are the tensor of intrinsic water and gas permeability, respectively, g the gravity acceleration, y the vertical, upward directed coordinate, and μ_w and μ_g the dynamic viscosity of the water and gas. The water permeability, assumed isotropic ($\mathbf{k}_w = k_w\mathbf{I}$, I, being the identity matrix), depends on the degree of saturation S_r according to the following equation:

$$k_w = k_{w,sat}S_r^{\,CKW1} \tag{8}$$

where $CKWI$ is a material parameter. $k_{w,sat}$ is the saturated permeability which depends on the soil porosity n through the Kozeni-Karman relation:

$$k_{w,sat} = k_{w0,sat}\frac{n^{EXPN}}{\left(1-n\right)^{EXPM}}\frac{\left(1-n_0\right)^{EXPM}}{n_0^{\,EXPN}} \tag{9}$$

where $k_{w0,sat}$ is the saturated water permeability corresponding to the reference porosity n_0 and $EXPN$ and $EXPM$ are material parameters of the Kozeny-Karman relation.

The dynamic viscosity of the water and gas are assumed linearly dependent on the temperature:

$$\mu_w = \mu_{w0}\left(1-\alpha_{w,T}\left(T-T_0\right)\right) \tag{10}$$

$$\mu_g = \mu_{g0}\left(1-\alpha_{g,T}\left(T-T_0\right)\right) \tag{11}$$

where μ_{w0} and μ_{g0} are the dynamic viscosity of water and gas, respectively, at initial temperature T_0. $\alpha_{w,T}$ and $\alpha_{g,T}$ are material parameters.

The velocity of water vapour diffusion is related to the air bulk density gradient:

$$\mathbf{i_v} = n\left(1-S_r\right)\tau D\rho_g\mathbf{grad}\left(\frac{\rho_a}{\rho_g}\right) \tag{12}$$

τ is the tortuosity of the material. D is the air diffusion coefficient depending on temperature and gas pressure:

$$D = 5.893\ 10^{-6}\frac{T^{2.3}}{p_g} \tag{13}$$

where D, T, and p_g are expressed in m^2/s, Kelvin, and Pascal, respectively.

The heat transport is governed by conduction and convection:

$$\mathbf{f_T} = -\Gamma\mathbf{grad}\left(T\right) + c_{p,w}\rho_w\mathbf{f_w} + c_{p,a}\left(\mathbf{i_a} + \rho_a\mathbf{f_g}\right) + c_{p,v}\left(\mathbf{i_v} + \rho_v\mathbf{f_g}\right) \tag{14}$$

where $c_{p,w}$, $c_{p,a}$ and $c_{p,v}$ are the specific heat of liquid water, dry air and water vapor. Γ is the thermal conductivity of the mixture as deduced from the thermal conductivity of each phase:

$$\Gamma = \lambda_s(1-n) + \lambda_w n S_r + \lambda_g n(1-S_r) \tag{15}$$

where λ_s, λ_w, and λ_a are the thermal conductivity of solid, liquid water, and gas phase, respectively.

The behaviour of the solid matrix is assumed to be governed by the generalized effective stress tensor $\boldsymbol{\sigma}'$ through combinations of mechanical stresses and fluid pressures (Bishop, 1961; Laloui & Nuth, 2009):

$$\boldsymbol{\sigma}' = \boldsymbol{\sigma} - p_g \mathbf{I} + S_r\left(p_g - p_w\right)\mathbf{I} \tag{16}$$

In this Lagrangian approach, the Cauchy strain tensor is used:

$$\boldsymbol{\varepsilon} = \frac{1}{2}\left(\mathbf{L} - \mathbf{L}^{\mathrm{T}}\right) \tag{17}$$

where $\mathbf{L} = \frac{\partial \mathbf{u}}{\partial \mathbf{X}}$ is the displacement ($\mathbf{u}$) gradient defined in the global axis ($\mathbf{X}$) in the moving current configuration (Charlier et al., 2001). This strain tensor is related to the generalized effective stress tensor through the mechanical constitutive model:

$$d\boldsymbol{\sigma}' = \mathbf{C} : d\boldsymbol{\varepsilon} \tag{18}$$

where $\mathbf{C}$ is the mechanical constitutive tensor.

2.3 *Mechanical constitutive model*

The mechanical model, called ACMEG-TS (François & Laloui, 2008), is based on an elasto-plastic framework, the total strain increment $d\boldsymbol{\varepsilon}$ being decomposed into non-linear, thermo-elastic, $d\boldsymbol{\varepsilon}^e$, and thermo-plastic, $d\boldsymbol{\varepsilon}^p$, components. The elastic part of the deformation is expressed as follows:

$$d\boldsymbol{\varepsilon} = \boldsymbol{E}^{-1} d\boldsymbol{\sigma}' - (1/3)\beta_s' \boldsymbol{I} dT \tag{19}$$

where $\mathbf{E}$ is the elastic tensor and β_s' the thermal expansion coefficient of the solid skeleton.

The plastic mechanism of the material is induced by two coupled hardening processes: an isotropic and a deviatoric one. Using the concept of multi-mechanism plasticity, both mechanisms may induce volumetric plastic strain (Hujeux, 1979). The yield functions of the two mechanical, thermo-plastic mechanisms have the following expressions (Figure 1):

$$f_{iso} = p' - p_c' \, r_{iso} \tag{20}$$

$$f_{dev} = q - Mp'\left(1 - b \; Log\frac{d\,p'}{p_c'}\right) r_{dev} = 0$$

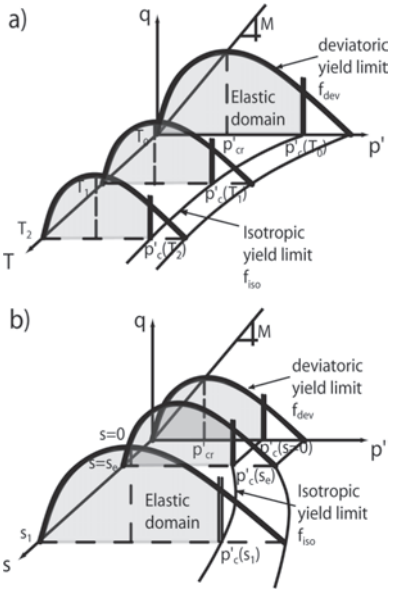

Figure 1. Effect of (a) temperature and (b) suction on the shape of coupled mechanical yield limits.

where p' is the mean effective stress, q the deviatoric stress and p_c' is the preconsolidation pressure. b, d and M are material parameters. p_c' depends on temperature T and suction s in addition to the volumetric plastic strain, $\boldsymbol{\varepsilon}_v^p$ (Salager et al., 2008):

$$p_c' = \begin{cases} p_{c0}' \exp\left(\beta\, \varepsilon_v^p\right)\left\{1 - \gamma_T \log\left[T/T_0\right]\right\}; & \text{if } s \le s_e \\ p_{c0}' \exp\left(\beta\, \varepsilon_v^p\right)\left\{1 - \gamma_T \log\left[T/T_0\right]\right\} & \\ \quad \left\{1 + \gamma_s \log\left[s/s_e\right]\right\}; & \text{if } s \ge s_e \end{cases} \tag{21}$$

where p_{c0}' is the initial preconsolidation pressure at ambient temperature T_0 and for suction lower than the air-entry value s_e. β is the plastic compressibility modulus and γ_T and γ_s are material parameters.

r_{iso} and r_{dev} are the degree of mobilization of the isotropic and the deviatoric mechanisms and are hyperbolic functions of the plastic strain induced by the isotropic and the deviatoric mechanisms, respectively (Laloui & François, 2009).

The details on the flow rules and the consistency conditions of both plastic mechanisms are detailed in François and Laloui (2008).

2.4 *Water retention constitutive model*

As long as the soil is drying, suction increases, and the degree of saturation S_r tends to decrease mainly when the air-entry suction s_e is reached. Under re-wetting, a hysteretic phenomenon occurs, also represented by a yielding process (Figure 2).

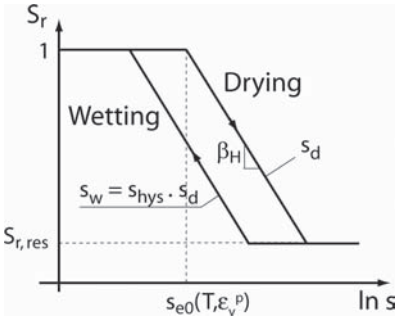

Figure 2. Schematic representation of water retention curve modelling: the hydraulic hysteresis. The amplitude of the hysteresis is governed by the s_{hys} parameter.

A wetting-drying cycle activates two successive yield limits in the ($S_r - s$) plane (f_{dry} and f_{wet}, along the drying and wetting paths, respectively):

$$f_{dry} = s - s_d = 0; \quad f_{wet} = s_d s_{hys} - s = 0 \tag{22}$$

where s_d is the drying yield limit and s_{hys} a material parameter considering the size of the water retention hysteresis. The drying limit s_d increases with the decrease of degree of saturation:

$$s_d = s_{d0} \exp\left(-\beta_h \, \Delta S_r\right) \tag{23}$$

where s_{d0} is the initial drying limit and β_h the slope of the desaturation curve in the (S_r – ln s) plane (Figure 2). s_{d0} is a function of temperature T and volumetric strain ε_v (François & Laloui, 2008):

$$s_d = s_{d0} \exp\left(-\beta_h \, \Delta S_r\right) \times \left\{1 - \theta_T \log\left[T/T_0\right] - \theta_e \log\left[1 - \varepsilon_v\right]\right\} \tag{24}$$

where θ_T and θ_e are material parameters describing the evolution of air-entry suction with respect to temperature and volumetric strain, respectively.

3 THE INFILTRATION TEST

3.1 *Presentation*

Non-isothermal infiltration tests through the bentonite, inside cylinders 60 cm in length and 7 cm in diameter, aim at simulating the water that saturates the barrier in a repository. A temperature of 100°C is imposed at the bottom of the cylinder while granitic water is injected at ambient temperature (20–30°C) under a pressure of 1.2 MPa over the upper lid of the cell (Lloret et al., 2004; Villar et al., 2005). The available measurements during the tests are temperatures at 50, 40, 30, 20 and 10 cm from the heaters and the volume of water intake. The duration of the tests has been 6, 12 and 24 months. After dismantling, the water content, as well as the dry density, at different locations was measured.

3.2 *Material characteristics*

The cylinders are filled with FEBEX bentonite blocks (Lloret et al., 2004). The THM properties of the FEBEX bentonite have been extensively investigated over the last decade (Villar, 1999; Lloret et al., 2003, Romero et al., 2005, among others).

A series of numerical simulations of oedometric tests on thermal, hydraulic and mechanical paths have been performed to calibrate the material parameters of the ACMEG-TS model (François & Laloui, 2008) (Figures 3 to 6; compression being positive) leading to the determination of the mecahnical and water retention parameters reported in Table 1. The tests performed by Lloret et al. (2004) start at an initial applied stress of 0.1 MPa and a compaction suction of about 127 MPa. Numerical simulations of oedometric compression tests at different suctions and ambient temperature are compared with experimental results in Figure 3 while Figure 4 reproduces the effect of oedometric compression tests for natural hydroscopic suction (127 MPa). Figure 5 reproduces the retention curve observed on wetting at three different temperatures and compares the results with numerical simulations. Figure 6 illustrates water retention hysteresis in addition to the effect of density.

The parameters governing the thermal and hydraulic diffusion in FEBEX bentonite are directly established from a literature synthesis. Villar (2002) reported the saturated hydraulic conductivity as a function of the dry density. Good agreements between Kozeni-Karman relation (Equation 9) and the evolution of permeability with dry density can be obtained for $k_{w0,sat} = 410^{-14} m/s$

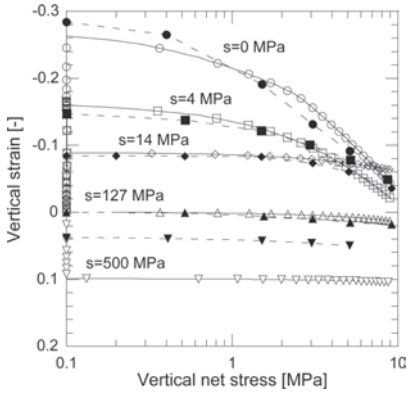

Figure 3. Numerical simulations (white points) of oedometric compressions on FEBEX bentonite at different suctions. Comparison with experiments (bold points).

Table 1. Set of the ACMEG-TS mechanical and water retention parameters for FEBEX bentonite.

Elastic parameters		
E_{ref}, ν, β_s'	[MPa], [-], [°C^{-1}]	9.78, 0.4, 6.67 10^{-4}
Isotropic plastic parameters		
β, γ_s, γ_T, p_c'	[-], [-], [-], [MPa]	14.3, 16.1, 2.1, 4
Deviatoric plastic parameters		
b, d, M, α	[-], [-], [-], [-],	1, 1.5, 1.2, 1
Water retention parameters		
s_{e0}, β_h, θ_T, θ_e, s_{hys}	[MPa], [-], [-], [-], [-]	4, 8.64, 0.7, 10.8, 0.6

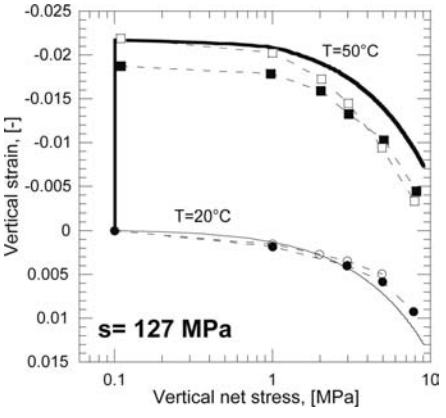

Figure 4. Numerical simulations (lines) of oedometric compressions on FEBEX bentonite at two different temperatures under a suction of 127 MPa. Comparison with experiments (dashed lines).

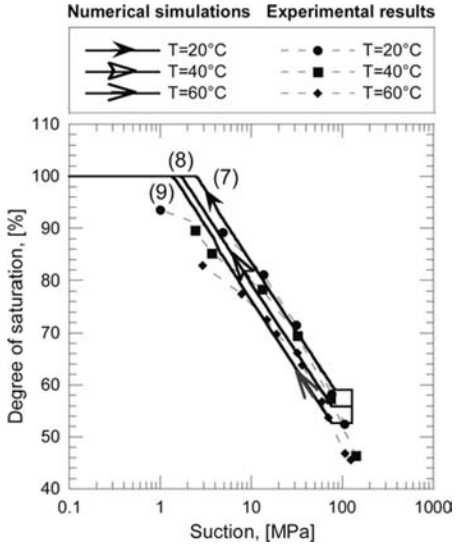

Figure 5. Numerical simulations of retention curves of FEBEX bentonite at different temperatures. Comparison with experiments.

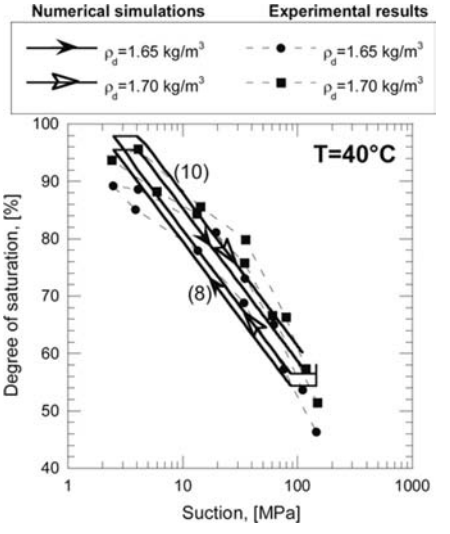

Figure 6. Numerical simulations of retention curves of FEBEX bentonite at two different dry densities. Comparison with experiments.

corresponding to $n_0 = 0.37$ (i.e. $\rho_d = 1.7 g/cm^3$) and $EXPN = EXPM = 6.5$ (Figure 7a).

In addition, the water permeability depends on the degree of saturation of the bentonite. Pintado et al. (2002) determined that $CKW1 = 2.9$. The thermal diffusion of each phase has been calibrated to reproduce the experimental evolution of the thermal diffusion of the bentonite with respect to its degree of saturation (λ_s; λ_w; λ_a) = (0.7; 2.1; 0) [$W/m°C$)] (Figure 7b). The heat capacity of the solid matrix is $c_s = 1091\ J/kg°C$ (Gens et al., 1998).

Table 2 reports the material parameters of FEBEX bentonite in relation to the thermal and hydraulic diffusion processes.

3.3 *Features of analysis*

The problem is treated under axisymmetric conditions around the longitudinal axis of the cylinder. The modelled domain, 3.5 cm in width

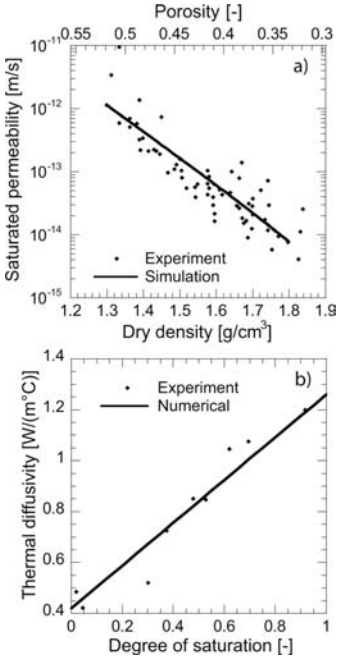

Figure 7. Effect of the degree of saturation on the thermal diffusivity of FEBEX bentonite. Comparison between laboratory measurements (Gens et al., 1998) and simulation.

and 60 cm long, is meshed with isoparametric elements. Gravity is not considered (Figure 8). The temperature is imposed at 100°C in the bottom of the cylinder which is assumed impervious. At the top of the cylinder, the pore water pressure is fixed to 1.2 MPa and the temperature is maintained as a constant. The thermo-hydraulic initial conditions have been imposed as follows: $T_0 = 23$°C; $s_0 = 127$ MPa; $S_{r0} = 0.54$.

Several disturbing effects related to the experimental procedures needed to be considered in the numerical simulations. The construction gaps as well as the deformability of the cell have been considered in the computations by imposing a progressive horizontal displacement of the lateral cylinder wall up to 1 mm after 24 months (Figure 8) in agreement with the measured overall decrease of the dry density from an initial value of 1.65 g/cm^3 to 1.57 g/cm^3 after 12-month and to 1.55 g/cm^3 after 24-month tests (Lloret et al., 2004).

As the cylinder is not insulated, the laboratory temperature has a non-negligible effect on the temperature distribution measured inside the cylinder. To consider this, radiation elements were introduced as thermal boundary conditions along the sample. A temperature of 23°C was fixed as the laboratory temperature and the emissivity ε of the cylinder (Teflon) was ascribed to 0.4. The thermal flux q_{rad} through radiation from the cylinder to the

Table 2. Material parameters of the diffusion processes in FEBEX bentonite. The parameters of the water retention curve are defined in Table 1.

Thermal parameters			
Solid thermal conductivity	λ_s	[W/(m°C)]	0.7
Water thermal conductivity	λ_w	[W/(m°C)]	2.1
Air thermal conductivity	λ_a	[W/(m°C)]	0
Solid heat capacity	$c_{p,s}$	[J/(kg°C)]	1091
Water heat capacity	$c_{p,w}$	[J/(kg°C)]	4200
Gas heat capacity	$c_{p,g}$	[J/(kg°C)]	1000
Liquid thermal expansion coefficient	β_w'	[°C^{-1}]	4 10^{-4}
Solid thermal expansion coefficient	β_s'	[°C^{-1}]	6.77 10^{-4}
Liquid dynamic viscosity thermal coefficient	$\alpha_{w,T}$	[°C^{-1}]	0.01
Hydraulic parameters			
Intrinsic waterpermeability	$k_{w0,sat}$	[m^2]	4 10^{-21}
Fluid dynamic viscosity	μ_w	[Pa · s]	0.001
Kozeni-Karman coefficient 1	$EXPM$	[–]	6.5
Kozeni-Karman coefficient 2	$EXPN$	[–]	6.5
Relative permeability coefficient	$CKW1$	[–]	2.9
Volumetric parameters			
Initial porosity	n_0	[–]	0.4
Solid specific mass	ρ_s	[kg/m^3]	2700
Water specific mass	ρ_w	[kg/m^3]	1000
Air specific mass	ρ_a	[kg/m^3]	1.18
Liquid compressibility	$1/\chi_w$	[Pa^{-1}]	3.33 10^{-10}

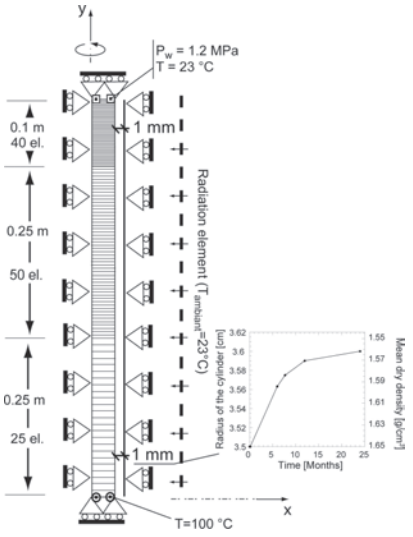

Figure 8. Finite element mesh used in the simulation of the infiltration test in FEBEX bentonite. The y-axis is the axis of symmetry of revolution.

laboratory is computed according to the Kirchhoff equation:

$$q_{rad} = \boldsymbol{\sigma}_{SB}\boldsymbol{\varepsilon}\left(T_{cyl}^4 - T_{lab}^4\right) \tag{25}$$

where T_{cyl} and T_{lab} are the temperatures of the cylinder and of the laboratory (T_{lab} = 23°*C*). σ_{SB} is the Stephan-Boltzmann constant (σ_{SB} = 5.67 10^{-8} W/(m^{2}K^4)).

Finally, the daily and seasonal temperature variation of the injected water, from 20°C to 30°C, has not been considered. An averaged temperature of 23°C was fixed at the top surface.

3.4 *Results*

Figure 9 compares the results of simulations with the experimental measurements in terms of temperature, water content and dry density distributions in the axis of the cylinder. First of all, the radiation elements, combined with accurate thermal diffusion and heat capacity of each phase of the bentonite, permit the reproduction of the sharp temperature decrease in the vicinity of the heater. At a location of 10 cm within the heater, simulations predict a temperature drop of 46.5°C (in comparison with 49°C, experimentally measured). Therefore, the thermal gradient is mainly concentrated in the bottom of the cylinder. The elevated temperature at the base of the cylinder produces an evaporation of water which diminishes the water content. In addition, that drying process induces shrinkage of the bentonite which

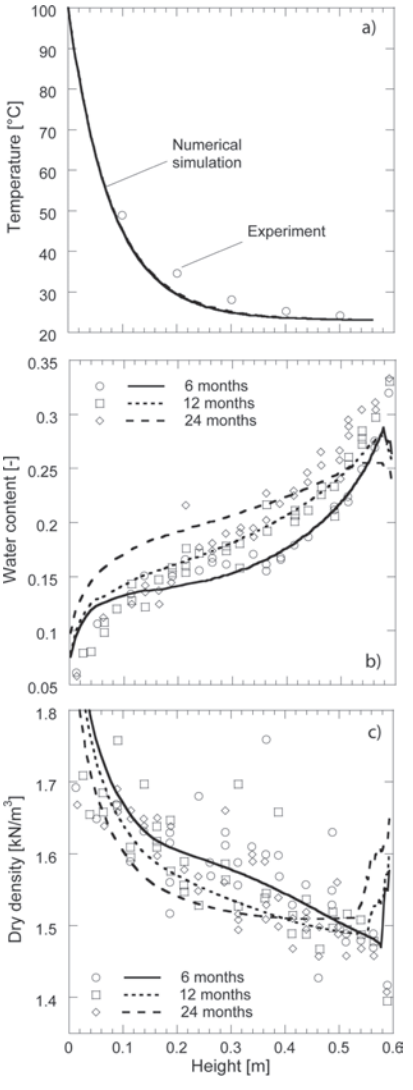

Figure 9. Results of the simulation of the infiltration test compared with experiment: a) Temperature distribution; b) Water content distribution; c) Dry density distribution.

is marked by an increase of the dry density at the bottom. On the contrary, at the top, the bentonite is wetted due to the water intake. That hydration process induces a swelling of the bentonite, except at the very top where numerical simulation predict a collapse phenomenon. The cooler region is also resaturated through the vapour that arises from the drying of the bottom part, migrates and condensates in the top part. In terms of water flux, the numerical simulation captures the main registered evolution of cumulative water intake (Figure 10).

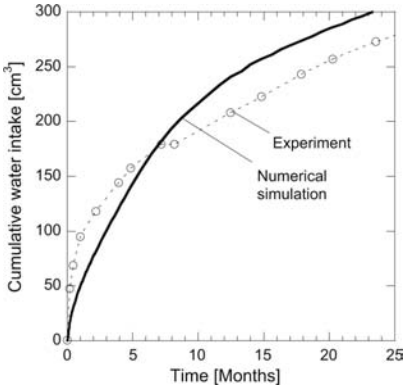

Figure 10. Evolution of cumulative volume of water intake. Comparison with experiment.

The good agreement validates the selected coefficient of permeability and its dependence with temperature, porosity and degree of saturation.

4 CONCLUSIONS

The numerical simulation of this infiltration test provides clear evidence of the ability of the used numerical tools to reproduce, from both the qualitative and quantitative viewpoints, the THM processes that occur in an engineered clay barrier. The THM behaviour of the FEBEX bentonite is well-documented in the literature. The results of accurate laboratory experiments were used to calibrate the model parameters through the numerical simulations of a series of oedometric tests. On the contrary, the parameters of the thermal and hydraulic diffusion models were extracted from the literature. The couplings between the thermo-hydraulic evolution and the mechanical response occurring in the cylinder have been underlined. It shows a combination of thermal and wetting expansion together with irreversible strains of the bentonite induced by hardening effects. This highly non-linear behaviour is a characteristic of the processes occurring in the engineered barrier of nuclear waste disposal.

REFERENCES

Bishop, A.W. 1959. The principle of effective stress. *Tecnisk Ukeblad*, 39: 859–863.

Charlier, R., Radu, J.P. & Collin, F. 2001. Numerical modelling of coupled transient phenomena. *Revue Française de Génie Civil*, 5(6): 719–741.

Collin, F. 2003. *Couplages thermo-hydro-mécaniques dans les sols et les roches tendres partiellement saturés*. PhD Thesis, University of Liège.

Collin, F., Chambon, R. & Charlier, R. 2006. A finite element method for poro mechanical modelling of geotechnical problems using local second gradient models. *International Journal of Numerical Methods in Engineering*, 65: 1749–1772.

Collin, F., Li, X., Radu, J.P. & Charlier, R. 2002. Thermo-hydro-mechanical coupling in clay barriers. *Engineering Geology*, 64: 179–193.

François, B. & Laloui, L. 2008. ACMEG-TS: A constitutive model for unsaturated soils under non-isothermal conditions. *Int. J. Num. Anal. Meth. Geomech*., 32: 1955–1988.

Gens, A., Garcia-Molina, A.J., Olivella, S., Alonso, E.E. & Huertas, F. 1998. Analysis of a full scale in-situ test simulating repository conditions. *Int. J. Num. Anal. Meth. Geomech*., 22: 515–548.

Hujeux, J.C. 1979. *Calcul numérique de problèmes de consolidation élastoplastique*. PhD Thesis, Ecole Centrale, Paris.

Laloui, L. & François, B. 2009. ACMEG-T: A soil thermo-plasticity model. *J. Eng. Mech*., 135(9), pp. 932–944.

Laloui L. & Nuth M. 2009. On the use of the generalised effective stress in the constitutive modelling of unsaturated soils. *Computer and Geotechnics*, 36 (1–2): 20–23.

Laloui, L., François, B., Nuth, M., Peron, H. & Koliji, A. 2008. A thermo-hydro-mechanical stress-strain framework for modelling the performance of clay barriers in deep geological repositories for radioactive waste. *Keynote lecture, Unsaturated Soils: Advances in Geo-Engineering*: 63–80.

Lloret, A., Romero, E. & Villar, M. 2004. FEBEX II Project: Final report on thermo-hydro-mechanical laboratory tests. *Publicación técnica 10/2004, ENRESA*.

Lloret, A., Villar, M., Sanchez, M., Gens, A., Pintado, X. & Alonso, E.E. 2003. Mechanical behaviour of heavily compacted bentonite under high suction changes. *Géotechnique*, 53: 27–40.

Pintado, X., Ledesma, A. & Lloret, A. 2002. Backanalysis of thermohydraulic bentonite properties from laboratory tests. *Engineering Geology*, 64: 91–115.

Romero, E., Villar, M. & Lloret, A. 2005. Thermo-hydro-mechanical behaviour of two heavily overconsolidated clays. *Engineering Geology*, 81: 255–268.

Salager, S., François, B., El Youssoufi, M.S., Laloui, L. & Saix, C. 2008. Experimental investigations on temperature and suction effects on compressibility and pre-consolidation pressure of a sandy silt. *Soils and Foundations*, 48(4): 453–466.

Villar, M. 1999. Investigation of the behaviour of bentonite by means of suction-controlled oedometer tests. *Engineering Geology*, 54: 67–73.

Villar, M. 2002. Thermo-hydro-mechanical characterisation of a bentonite from Cabo de Gata: A study applied to the use of bentonite as sealing material in high level radioactive waste repositories. *Publicación técnica 04/2002, ENRESA*.

Villar, M., Garcia-Sineriz, J.L., Barcena, I. & Lloret, A. 2005. State of the bentonite barrier after five years operation of an in-situ test simulating a high level radioactive waste repository. *Engineering Geology*, 80: 175–198.